Eur Biophys J (1997) 26: 283–290

ARTICLE

M. Benoit · T. Holstein · H. E. Gaub

Lateral forces in AFM imaging and immobilization of cells and organelles

Received: 11 March 1996 / Accepted: 23 April 1997

Abstract Lateral forces are inevitable in contact mode AFM imaging and they contribute significantly to the image formation under certain conditions. In cases where the objects are comparable in size to the cantilever tip and particularly in cases where the tips have a high aspect ratio, the lateral force may exceed the vertical force and may impose a severe limitation to the stability of the sample during imaging. Here we have calculated the relation between the exerted lateral force and the applied vertical force as a function of the friction coefficient, the geometry of the tip, and the stiffness of the cantilever. We present a strategy to immobilize larger particles by sucking them into the pores of nucleopore filters and binding them by chemical cross linking. High resolution images of nematocysts which were immobilized with this strategy are presented. The images reveal the supra-molecular arrangement of the minicollagen of the capsule wall.

Key words AFM · Lateral forces · Nucleo-pore filter · Immobilization · Nematocysts

Introduction

The AFM has evolved into an extremely useful new instrument for the in-situ and in-vivo investigation of biological samples (Hoh and Schoenenberger 1994; Radmacher et al. 1992; Hansma and Hoh 1994; Engel 1991). DNA (Bezanilla et al. 1994; Shaper et al. 1993), proteins (Weisenhorn et al. 1990; Müller et al. 1996) and supported membranes (Tillmann et al. 1993; Egger et al. 1990) have been imaged with stunning resolution. Individual molecular actions (Radmacher et al. 1994) and interactions have been investigated (Florin et al. 1994; Moy et al. 1994; Lee et al. 1994; Dammer et al. 1995). The option to operate in real time under quasi physiological conditions has opened new possibilities, particularly in cell research (Henderson et al. 1992; Schoenenberger and Hoh 1994; Fritz et al. 1994; Radmacher et al. 1992). Novel instruments and especially adapted operation modes have helped to overcome the initial difficulties, which arose mainly from the high lateral and normal forces between tip and cell (Putman et al. 1992; Hansma et al. 1994; Butt et al. 1992). Today, normal forces can be as low as a few tens of pN, a value which in the case of flat, extended cells allows non-invasive imaging over prolonged time spans. In the case of round massive cells or organelles, however, the high lateral forces still hamper stable imaging. The influence of lateral forces on protein imaging and strategies to overcome these specific difficulties have already been discussed in several papers (Weisenhorn et al. 1990; Bezanilla et al. 1994; Aimé et al. 1994; Kasas and Ikai 1995). Here we will focus on the interaction between the tip and objects which are large compared to the curvature radius of the tip.

M. Benoit · H. E. Gaub (✉)
Sektion Physik, Ludwig-Maximilians-Universität,
D-80977 München, Germany

T. Holstein
Zoologisches Institut, J. W. Goethe Universität,
D-60590 Frankfurt a. Main, Germany

Theory of imaging forces

I Lateral forces when scanning large objects

The mechanism that gives rise to the high lateral and normal forces can easily be rationalized with the help of the schematic drawing in Fig. 1. In the case of macroscopic objects which are large compared to the curvature radius of the tip, the leading lateral force between object and tip arises from the contact of the object with the side of the tip rather than with the apex. This kind of contact is unfavorable for high resolution imaging but typically occurs when the sample is screened at low magnifications. The lateral force between tip and object is not only a function of the vertical force, but depends strongly on the aspect ratio, the tilt angle of the cantilever, and the friction coefficient

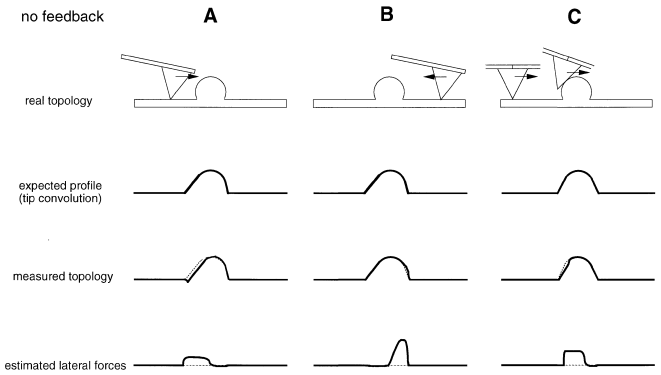

Fig. 1 A–C Cartoon of the AFM tip and the torsion of the cantilever scanning a macroscopic object in different directions with no feedback. Also schematically shown are the lateral forces and the resulting image distortions

between tip and object. Via the effective tip length, this lateral force exerts a torque onto the cantilever which causes, depending on the relative orientation, either a bend, (Fig. 1 a, b) or a twist (Fig. 1 c) of the cantilever. A detailed calculation of this problem is given in the appendix. The force balance results in a non-analytical expression which was numerically solved following standard procedures (see appendix). The result is given in Fig. 2, where the normalized lateral force is plotted as a function of the contact angle of the tip, α (aperture angle plus tilt angle) for different friction coefficients, μ, and different effective cantilever stiffness, ν. The plots reveal that the lateral force is a sensitive function of the friction coefficient (Fig. 2 a, b) and the aspect ratio (Fig. 2 c, d).

In the case of tips with a large aspect ratio, the lateral force is rather insensitive to the cantilever stiffness (Fig. 2 a, b). Only in the case of tips with a high aspect ratio, like the electron beam deposited carbon tips, does the stiffness of the cantilever play a dominant role (Fig. 2 c, d). It is interesting to note that in a typical case, where we use an integrated tip with an angle of 30 degrees on a soft cantilever with $d/\nu \cdot l^2 = 0.0001\ N^{-1}$, the lateral force is already more than twice the vertical force even with an extremely low friction coefficient of 0.01. With a moderate value for the friction coefficient of 0.4 and a typical cantilever stiffness $\nu = 0.04$ Nm resulting in $d/\nu \cdot l^2 = 0.01\ N^{-1}$, the lateral force exceeds the vertical force by an order of magnitude! In the case of carbon tips the situation is even more dramatic.

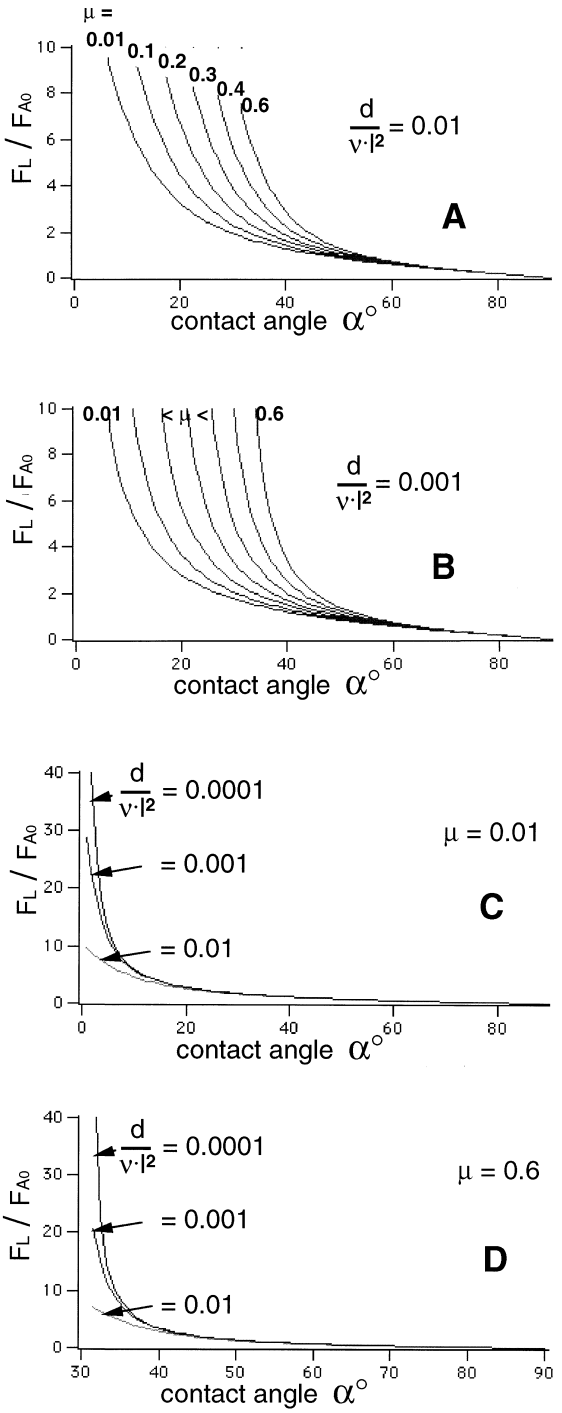

Fig. 2 A–D Calculated lateral forces in constant height mode (no feedback) between an AFM tip and a spherical object with different friction coefficients, μ (**A** and **B**), and different normalized cantilever stiffness, $d/\nu \cdot l^2$ (**C** and **D**), as a function of the contact angle, α, between tip and object

II Lateral forces in feedback modes

In order to avoid excessive loads, imaging of cells typically occurs in either the constant force mode or in the so-called error signal mode (Putman et al. 1992). In both cases the deflection of the cantilever is compensated by raising or lowering the sample or the cantilever. As depicted schematically in Fig. 3 the lateral forces may contribute significantly (via the bend of the cantilever) to the deflection of the cantilever, so that a compensation of the deflection via the height signal may result in excessive lateral and vertical forces. This is particularly the case in the situation that is sketeched in Fig. 3 a. Here the lateral force leads to an additional tilt which results in a signal on the split photo

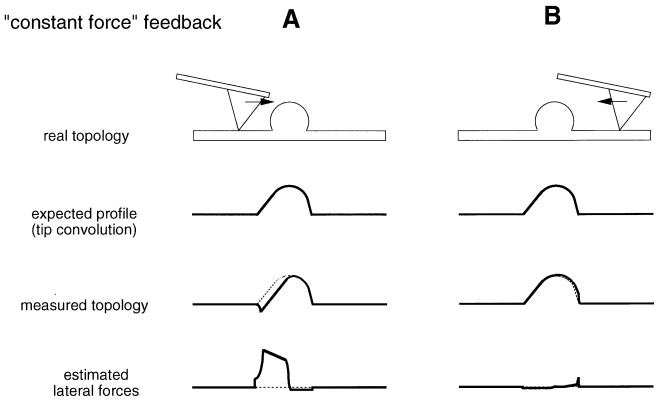

Fig. 3 A, B Cartoon of the lateral forces and the resulting distortions in the case of the constant deflection feedback generally referred to as "constant force mode" (the resulting lateral forces are highly dependent on details of the feedback settings)

detector which is equivalent to that of a lower z position. The compensation in this case will increase the load by raising the sample and thus even further increase the bend. In the opposite scan direction, however, lateral forces tend to reduce the applied load. In this scan direction the feedback will actually overcompensate the friction force so that the resulting lateral forces should be the lowest possible. A detailed calculation of this effect is given in the appendix. Figure 4 gives the results of the numerical simulation. Figure 4 a, b show, for the case of the forward scan, the ratio of the lateral to the normal force as a function of the tip apex for different friction coefficients. Figure 4 a, b differ in the length of the cantilever. The graphs reveal that even at moderate friction coefficients the lateral forces may exceed the normal forces by an order of magnitude for tips with a small apex angle. In the case of the backwards scan, Fig. 4 c, d reveal that the maximum lateral forces are limited and significantly lower than in the case of the forward scan. The limit is interestingly not a function of the friction coefficient and the apex angle but depends only on the cantilever parameters and the tip length. This means that when scanning large objects this scan direction should be chosen for imaging and the tip should be retracted completely during the forward scan. If the scan direction is chosen perpendicular to the cantilever symmetry axis, both back and forth scans are symmetric. In this case, however, the lateral force acts equally and cannot be compensated directly.

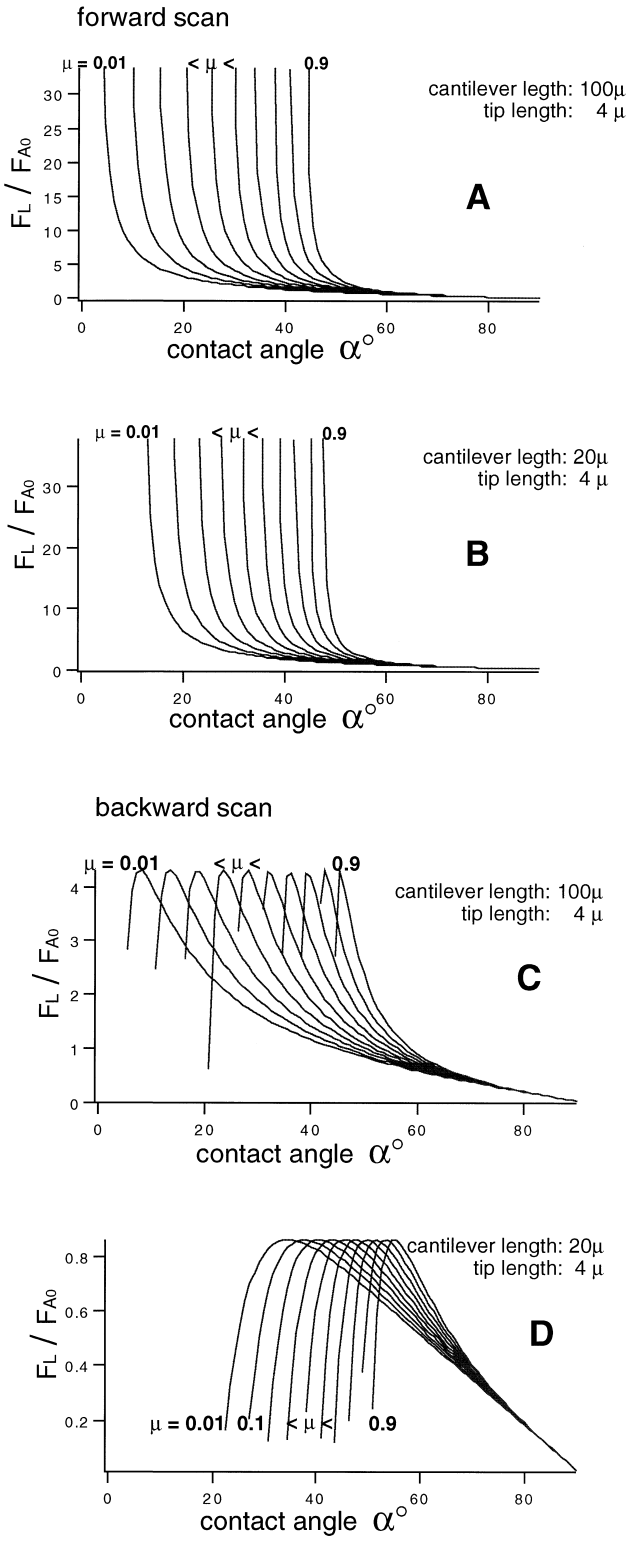

Fig. 4 A–D Calculated lateral forces with feedback ("constant force mode") as a function of the contact angle, α, for different friction coefficients, μ (0.01; 0.1; 0.2; 0.3; …; 0.8; 0.9), for a long (**A** and **C**) and a short cantilever (**B** and **D**), in forward (**A** and **B**) and backward (**C** and **D**) scan direction

Materials and methods

I Instrumentation

For AFM-imaging a Nanoscope III (Digital Instruments) with a J-scanner was used. Standard silicon nitride cantilevers (k = 32 mN/m) with carbon tips, grown in a scanning electron microscope, were used (Keller and Chih-

Chung 1992). All experiments were carried out in a fluid-cell in order to keep the sample under aqueous conditions. The images have a format of 256×256 pixels 16 Bit each. The scan angle was 90° (horizontal). The scan speed varied between 3 and 100 lines/s. The integral gain and the setpoint were adjusted such that the imaging force was kept as low as possible.

II Isolation of nematocysts

Nematocysts from whole freshwater hydras were isolated as follows: between 100 to 1000 animals – starved for 24 h – were frozen at –20 °C for 30 min. After warming up to 4 °C all cellular tissue, except for the nematocysts, was destroyed. The centrifugation at 1000×g in a Percoll-gradient of 1,20 g/mol at 4 °C separates the capsules in the pellet with a density of 1,24 g/mol from the rest. The purified capsules were resuspended in a 2 N NaCl solution. For more details see Weber et al. (1987) and Benoit et al. (1995).

III Immobilization of the capsules

As was pointed out in the theory section, the lateral force between tip and cell makes a suitable immobilization of the organelles or cells to be imaged essential. As a result of various experiments with different immobilization strategies, we found the approach, outlined in Fig. 5, to be the most successful (also reported by Kasas and Ikai (1995)). Nucleopore filters (e. g. Costar, Tübingen Germany) with holes in the range of the size of the cells or organelles are first coated with gelatin by immersing them in a solution of 1% gelatin for a few minutes and drying them afterwards in ambient air. The dried filters are then soaked in a 25% glutaraldehyde solution for 20 minutes and carefully rinsed with Millipore water. Now the filters are placed in a filter holder connected to a suction pump. The organelle suspension is gently sucked through the filter. Organelles that are not sucked into the pores may afterwards be removed with a little wheelbarrow or by wheeling the filter surface after filtering and washing softly with the filter medium. For successful AFM imaging this removal of unattached organelles turned out to be very important as the loose organelles tend to stick to the cantilever and as a result smear out the image. Since the nucleopore filters are translucent, one may easily control the preparation in the light microscope. For AFM imaging, the filters are kept in the medium and placed on the sample holder by water insoluble double stick tape (e.g. tesafix 4972). As an example, Fig. 6 a, b show a nucleopore filter before and after nematocysts have been aspirated into the pores. The major advantages in immobilizing the organelles by aspirating them into the pores of nucleopore filters are that such filters are flat, that they are available with different pores sizes and that the pore diameters have a rather narrow distribution The latter is important for a high yield, a fact which, in view of the limited scan range of the AFM, should not be underestimated. We found that the treatment of the filters with gelatin and glutaraldehyde is not essential but it helped to increase the number of nematocysts which are stably immobilized. Since the thorough washing removed free glutaraldehyde, we assume that this immobilization is caused by adhesion of the organells to the crosslinked gelatin rather than by chemical fixation. Unless otherwise noticed all chemicals were purchased from Sigma.

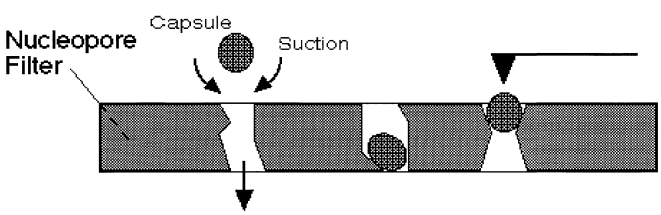

Fig. 5 Schematic of the immobilization of cells or organelles in the pores of a nucleopore filter

Results and discussion

Like other Cnidarians, the freshwater polyp *Hydra* has stinging cells which are used for the capture and poisoning of prey. These stinging cells contain explosive capsules called *nematocysts* which are 5 to 15 μm in diameter and are charged with an osmotic pressure of up to 150 bar (Weber 1989). This enormous pressure is maintained by the cell wall whose main constituent is a special type of collagen (Petri 1991). It was the goal of this study to investigate the molecular organization of the collagen in the nematocyst capsule wall by AFM (Holstein et al. 1994). The theoretical considerations concerning lateral forces, that were presented in the first part of the paper, evolved during the initial phase of the project, where attempts had failed to image these organelles when they were just adsorbed onto different supports which were successfully used for samples like proteins (Radmacher et al. 1994). On a regular basis, the organelles were removed from the surface or laterally displaced by the cantilever after a few scans. As a result, we developed the immobilization strategy described above and found that capsules and also intact cells (results not shown here) that were trapped in the holes of the nucleopore filter, may be stably imaged for hours. Figure 6 c shows the AFM image of a capsule caught in a pore. Owing to the large size of the object, one can clearly see the convolution of the tip geometry with the sample. When the integrated pyramid of the cantilever interacts with the sides of the nematocyst, the image reflects mainly the geometry of the tip. It is in these areas of the image where the highest lateral forces act between tip and sample, as we have pointed out in the theory section of this paper. Only in the center part, where the carbon tip interacts with the upper part of the nematocyst, is the image dominated by the sample texture. Here the structure of the capsule wall can be imaged with high resolution.

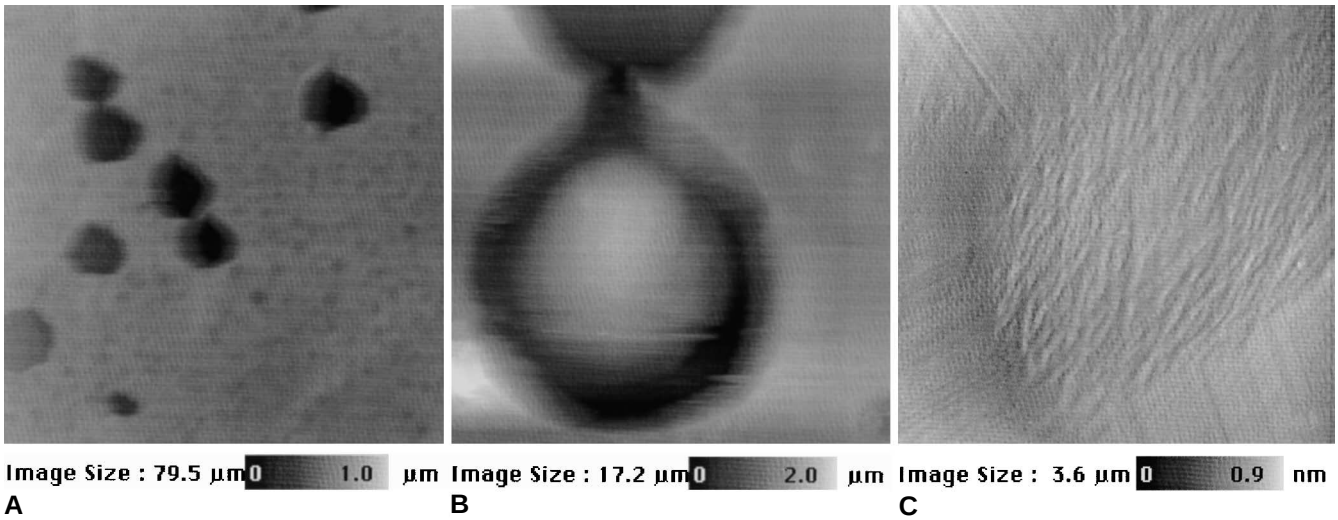

Fig. 6 AFM image of a nucleopore filter before (**A**) and after (**B**) aspiration of nematocysts; **C** close-up view of a nematocyst in deflection mode (note the tip convolution) (Imaging conditions: Nanoscope III, J-scanner; silicon nitride cantilevers k = 32 mN/m 256×256 pixels, scan angle 90°, scan speed: 5 lines/sec, integral gain = 1, **A** and **B** carbon tip, constant height mode, **C**: no carbon tip, deflection mode)

In order to resolve the supra molecular arrangement of the molecular constituents of the capsule wall we have recorded a series of high resolution images from different nematocysts. Figure 7 a shows an example, where the fibers form a whirl like structure which was not resolved with other techniques. This supra molecular arrangement of the fibers is typical for the polar area of the capsule. At higher magnification in Fig. 7 b the streaky substructure of the fibers is revealed.

The fibers are 50 to 120 nm wide and the stripe pattern has an average periodicity of 32 nm. Imaging at this resolution was possible for several tens of minutes without noticeable change in the structure and without displacement of the sample, confirming the quality of the immobilization. Type 1 collagen, the main constituent of mammal tendons, has AFM images which reveal a structure with a diameter of 280 nm and a periodicity of about 60 nm with a sub pattern of micro fibrils of 5 nm (Baselt et al. 1993). In contrast, the minicollagenes of the Hydra N-Col 1, 2, 3 and 4 (Petri 1991) which are procollagenes, form a finer pattern which is probably better adapted to the special purpose of the organelles. The pattern found in Hydra also suggest that the intermolecular bonding differs considerably in both systems.

Concluding remarks

When imaging objects with the AFM that are comparable in size with the tip, lateral forces play a key role. In particular, tips with a low apex angle, that are preferable for

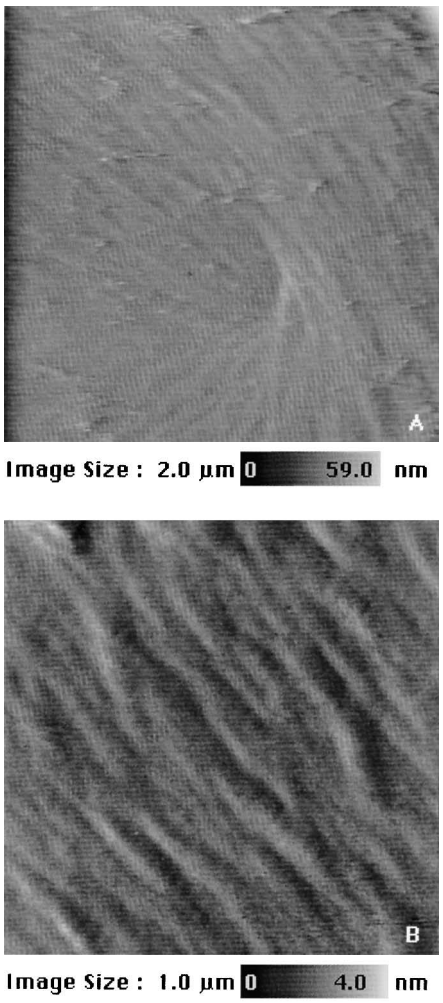

Fig. 7 A, B Zoom series on the capsule wall of a nematocyst. (Imaging conditions: same as in Figs. 6 A, B, except deflection-mode, integral gain = 0.031)

their high resolution, give rise to lateral forces that may easily exceed the normal forces by orders of magnitude. For stable imaging the immobilization of the sample is therefore essential. In the case of large, round shaped objects like cells or organelles, capture in nucleopore filters has proven to be a practical and very reliable technique. This technique allowed us to stably image the supra molecular structure of nematocyst capsule walls at high resolution over extended periods of time.

Acknowledgements This work was supported by the Deutsche Forschungsgemeinschaft. Helpful discussions with Monika Fritz and technical support from Digital Instruments are gratefully acknowledged. The tips were grown in the laboratory of Andreas Engel.

Appendix

I Lateral forces in constant height mode

In order to calculate the lateral force, we first consider geometrical aspects, then introduce friction, and finally include the bending stiffness of the cantilever. Depending on the chosen setpoint the tip applies a certain vertical force F_A to the object. Taking the geometrical relations depicted in Fig. 8 a the lateral force is given by:

$$F_{L_0} = \frac{F_A}{\tan\alpha} \tag{1}$$

This gives rise to the normal force F_{N_0}:

$$F_{N_0} = \frac{F_A}{\sin\alpha} \tag{2}$$

If we introduce friction with μ as coefficient this normal force results in the friction force:

$$F_{R_0} = \mu \cdot F_{N_0} \tag{3}$$

In order to overcome this frictional force F_{R_0} an additional lateral force F_{L_0} is required, which in turn increases the frictional force by F_{R_1} and so on (see Fig. 8 a). The effective lateral force will therefore be the sum over all contributions F_{R_j}. Equation (3) can be generalized for all contributions by introducing the indices, j:

$$F_{R_j} = \mu \cdot F_{N_j} \tag{4}$$

Successively one obtains for the normal forces:

$$F_{N_{j+1}} = \frac{F_{R_j}}{\tan\alpha} \tag{5}$$

This yields the iteration rule:

$$F_{R_{j+1}} = \frac{\mu}{\tan\alpha} F_{R_j} \tag{6}$$

which can be transformed into:

$$F_{R_j} = \left(\frac{\mu}{\tan\alpha}\right)^j F_{R_0} = \left(\frac{\mu}{\tan\alpha}\right)^j \frac{\mu \cdot F_A}{\sin\alpha} \tag{7}$$

For the lateral force holds then the relation:

$$F_{L_{j+1}} = \frac{F_{R_j}}{\sin\alpha} \tag{8}$$

With Eq. (7) this results in:

$$F_{L_{j+1}} = \left(\frac{\mu}{\tan\alpha}\right)^j \frac{\mu \cdot F_A}{\sin^2\alpha} \tag{9}$$

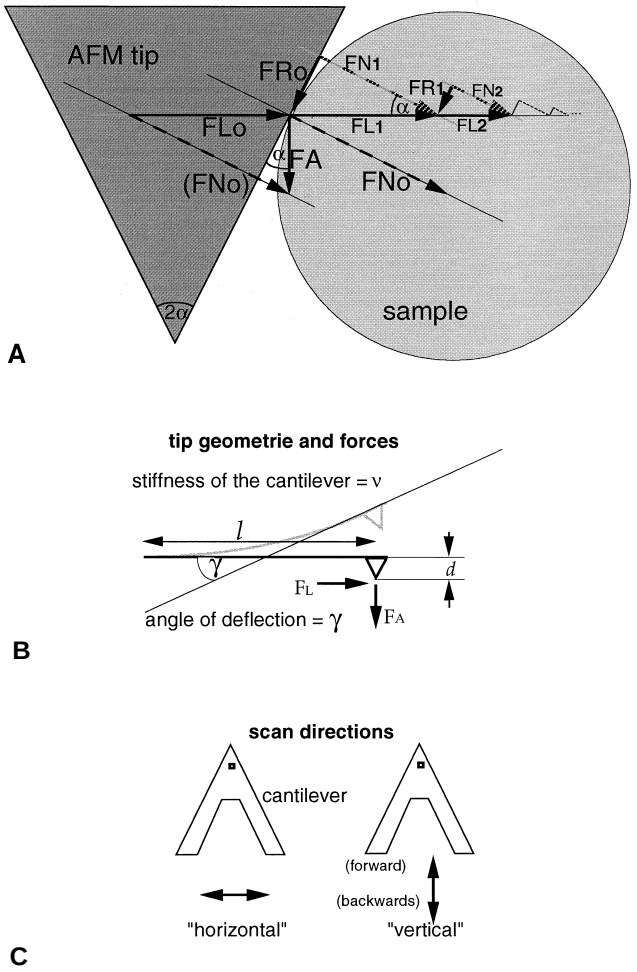

Fig. 8 **A** Schematics of the interaction of the AFM tip with a macroscopic object. Outlined are the normal force and the resulting lateral force. **B** Schematics of the bend of the cantilever and the definition of the angle γ. **C** Definitions of forward and backward scan directions

The effective lateral force, $F_{L_{eff}}$, is now obtained by summing over all contributions F_{L_j} to the lateral force:

$$F_{L_{eff}} = \sum_{j=0}^{\infty} F_{L_j} = \frac{F_A}{\tan\alpha} + \frac{\mu \cdot F_A}{\sin^2\alpha} \sum_{j=0}^{\infty} \left(\frac{\mu}{\tan\alpha}\right)^j \tag{10}$$

$$F_{L_{eff}} = \frac{F_A}{\tan\alpha}\left(1 + \frac{\mu \cdot \cos\alpha}{\tan\alpha - \mu}\right) \tag{11}$$

The summation is only valid if μ is smaller than tan α, a condition which is always fulfilled if the cantilever can bend.

As a result of the lateral force the tip will exert a torque on the cantilever which will result in a tilt of the tip. The bend will enlarge the effective tip angle

$$F_{L_{eff}} = \frac{F_A}{\tan\varepsilon}\left(1 + \frac{\mu \cdot \cos\varepsilon}{\tan\varepsilon - \mu}\right) \tag{12}$$

With a stiffness, ν, and a length, l, of the cantilever and a tip length, d, the bend angle is then given by:

$$F_A = \tan(\gamma) \cdot \nu \cdot l\,, \quad F_L = \tan(\gamma) \cdot \nu \frac{l^2}{d} \tag{13}$$

This results in the following non-analytical relation for the effective lateral force:

$$\frac{F_{L_{eff}}}{F_A}\cdot\tan\left(\alpha+\arctan\left(F_{L_{eff}}\,\frac{d}{l^2\cdot\nu}\right)\right)+\frac{\mu\cdot\cos\left(\alpha+\arctan\left(F_{L_{eff}}\,\frac{d}{l^2\cdot\nu}\right)\right)}{\mu-\tan\left(\alpha+\arctan\left(F_{L_{eff}}\,\frac{d}{l^2\cdot\nu}\right)\right)}=1 \quad (14)$$

Numerical solutions of this equation were calculated by iteration. The results are plotted in Fig. 2.

II Lateral forces in constant force mode

In the so called constant force mode, the feedback loop of the AFM is programmed such that it keeps the deflection of the beam constant by regulating the z-position. Since the contribution of the lateral forces to the cantilever torsion, and by means of this to the beam deflection, depends on the scan direction, this compensation strategy leads to largely varying forces. In the ideal case where scanning perpendicularly to the symmetry axis of the cantilever results only in a torsion along this axis, the lateral force will not contribute to a deflection signal. The triangular geometry and the off axis position of the tip, however, will always cause an additional torsion in other directions. For simplicity we discuss here only the extreme case where the cantilever is scanned back and forth parallel to the symmetry axis of the cantilever. In this case the tilt angle, δ, of the cantilever adds to (forward) or subtracts from (backward) the tip angle, so that Eq. (14) converts into:

$$\frac{F_{L_{eff}}}{F_A}\cdot\tan\left(\alpha\pm\delta+\arctan\left(F_{L_{eff}}\,\frac{d}{l^2\cdot\nu}\right)\right)+\frac{\mu\cdot\cos\left(\alpha\pm\delta+\arctan\left(F_{L_{eff}}\,\frac{d}{l^2\cdot\nu}\right)\right)}{\mu-\tan\left(\alpha\pm\delta+\arctan\left(F_{L_{eff}}\,\frac{d}{l^2\cdot\nu}\right)\right)}=1 \quad (15)$$

For a constant deflection γ_0 this equation reduces to

$$F_{L_{eff}}=\frac{F_A}{\tan(\alpha_+ +\arctan(\gamma_0))}\left(1+\frac{\mu\cdot\cos(\alpha_+ +\arctan(\gamma_0))}{\tan(\alpha_+ +\arctan(\gamma_0))-\mu}\right) \quad (16)$$

where γ_0 is defined by the setpoint and results in a the vertical force F_{A_0}:

$$F_{A_0}=\tan(\gamma_0)\cdot\nu\cdot l \quad (17)$$

Note that the argument of the tangent must not exceed $\Pi/2$ and that μ must not exceed $\tan(\alpha_+ +\arctan(\gamma_0))$. Beyond these limits the approximation of the cantilever as a thin beam does not hold any more. Equation (16) may be abbreviated as:

$$F_{L_{eff}}=F_A\cdot C(\gamma_0) \quad (18)$$

where the constant C, is only determined by the setpoint, the friction coefficient, and the experimental geometry. What we need is to find an expression for F_A.

During forward scan the vertical force, F_{A_0}, causes a lateral force, $F_{L_{eff\,0}}$, which tries to bend the cantilever such that deflection is decreased. The feedback compensates for this by raising the sample, which gives rise to an additional vertical force, F_{A_1}. This addition vertical force gives rise to an additional lateral force, $F_{L_{eff\,1}}$, which in turns tries to increase the deflection again. In analogy to the previous chapter, this can be described by the following recursion algorithm:

$$F_{L_{eff\,j}}=F_{A_j}\cdot C(\gamma_0)\quad\text{and}\quad F_{A_{j+1}}=C(\gamma_0)\,\frac{d}{l}\cdot F_{A_j} \quad (19)$$

The overall force is thus the sum of all partial forces.

$$\begin{aligned}F_{L_{eff}}&=F_{L_0}\pm\sum_{j=1}^{\infty}F_{L_j}=F_{L_0}\pm C\cdot F_{A_0}\sum_{j=1}^{\infty}\left(\frac{C\cdot d}{l}\right)^j\\&=C\cdot F_{A_0}\pm\left[C\cdot F_{A_0}\sum_{j=1}^{\infty}\left(\frac{C\cdot d}{l}\right)^j-C\cdot F_{A_0}\right]\\&=C\cdot F_{A_0}\left[1\pm\left(\frac{l}{l-C\cdot d}-1\right)\right]\\&=C\cdot F_{A_0}\left(1\pm\frac{C\cdot d}{l-C\cdot d}\right)=C\cdot F_{A_0}\left(1\pm\frac{l}{\frac{l}{C\cdot d}-1}\right)\forall_{l>C\cdot d}\end{aligned} \quad (20)$$

The + holds for the forward scan and the – holds for the backward scan were the feedback reduces the forces. This equation was solved numerically again. The results are plotted in Fig. 4.

References

Aimé JP, Elkaakour Z, Gauthier S, Curély J, Bouhancina T, Odin C (1994) Role of the the friction on curved surfaces in scanning force microscopy. Surface Science 329: 149 – 156

Baselt DR, Revel J-P, Baldeschwieler JD (1993) Subfibrillar structure of type I collagen observed by atomic force microscopy. Biophys J 65: 2644 – 2655

Benoit M, Holstein T, Gaub HE (1995) In: Colton R, Engel A, Frommer J, Gaub HE, Gewirth A, Guckenberger R, Heckl W, Parkinson B, Rabe J (eds) Procedures in Scanning Probe Microscopies. Wiley, Sussex

Bezanilla M, Drake B, Nudler E, Kashlev M, Hansma PK, Hansma HG (1994) Motion and enzymatic degradation of DNA in the atomic force microscope. Biophys J 67: 1 – 6

Butt HJ, Guckenberger R, Rabe JP (1992) Quantitative scanning tunneling and scanning force microscopy of organic materials. Ultramicroscopy 46: 357 – 359

Dammer U, Popescu O, Wagner P, Anselmetti D, Güntherodt H-J, Misevic GN (1995) Binding strength between cell adhesion proteoglycans measured by atomic force microscopy. Science 267: 1173 – 1175

Egger M, Ohnesorge F, Weisenhorn A, Heyn SP, Drake B, Prater CB, Gould SAC, Hansma P, Gaub HE (1990) Wet lipid-protein membranes imaged at submolecular resolution by atomic force microscopy. J Struct Biol 103: 89 – 94

Engel A (1991) Biological applications of scanning probe microscopes. Annu Rev Biophys Biophys Chem 20: 79 – 108

Florin E-L, Moy VT, Gaub HE (1994) Adhesion forces between individual ligand-receptor pairs. Science 264: 415 – 417

Fritz M, Radmacher M, Gaub HE (1994) Granula motion and membrane spreading on human platelets imaged with the AFM. Biophys J 66: 1 – 7

Hansma HG, Hoh JH (1994) Biomolecular imaging with the atomic force microscope. Annu Rev Biophys Biomol Struct 23: 115 – 139

Hansma PK, Cleveland JP, Radmacher M, Walters DA, Hillner PE, Bezanilla M, Fritz M, Vie D, Hansma HG, Prater CB, Massie J, Fukunaga L, Gurley J, Elings V (1994) Tapping mode atomic force microscopy in liquids. Appl Phys Lett 64: 1738 – 1740

Henderson E, Haydon PG, Sakaguchi DS (1992) Actin filament dynamics in living glial cells imaged by atomic force microscopy. Science 257: 1944 – 1946

Hoh JH, Schoenenberger C-A (1994) Surface morphology and mechanical properties of MDCK monolayers by atomic force microscopy. Biophys J 107: 1105 – 1114

Holstein TW, Benoit M, Herder G v, Wanner G, David C, Gaub HE (1994) AFM reveals fibrous mini-collagens in hydra nemtocysts. Science 265: 402 – 404

Kasas S, Ikai A (1995) A new method for anchoring round shaped cells for atomic force microscope imaging. Biophys J 68: 1678 – 1680

Keller D, Chih-Chung C (1992) Imaging steep, high structures by scanning force microscopy with electron-beam deposited tips. Surf Sci 268: 333 – 339

Lee GU, Chris LA, Colton RJ (1994) Direct measurement of the forces between complementary strands of DNA. Science 266: 771 – 773

Moy VT, Florin EL, Gaub HE (1994) Intermolecular forces and energies between ligands and receptors. Science 266: 257 – 259

Müller DJ, Schoenenberger CA, Büldt G, Engel A (1996) Immuno atomic force microscopy of purple membrane. Biophys J 70: 1796 – 1802

Petri B (1991) Biochemische und immunochemische Charakterisierung der Kapselwand von Nematozysten bei Hydra. (Zoologisches Institut Ludwig-Maximilian-Universität München, Diploma thesis)

Putman CA, Werf KO vd, Grooth BG d, Hulst NF v, Greve J, Hansma PK (1992) A new imaging mode in Atomic Force Microscopy based on the error signal. Proc Soc Photo-Opt Instrum Eng 1639: 198 – 204

Radmacher M, Fritz M, Hansma HG, Hansma PK (1994) Direct observation of enzyme activity with the atomic force microscope. Sicence 265: 1577 – 1579

Radmacher M, Tillmann RW, Fritz M, Gaub HE (1992) From molecules to cells – imaging soft samples with the AFM. Science 257: 1900 – 1905

Schoenenberger CA, Hoh JH (1994) Slow cellular dynamics in MDCK and R5 cells monitored by time-lapse atomic force microscopy. Biophys J 67: 929 – 936

Shaper A, Pietrasanta LI, Jovin TM (1993) Scanning force microscopy of circular and linear plasmid DNA spread on mica with a quaternary ammonium salt. Nucleic Acids Research 21: 6004

Tillmann RW, Radmacher M, Gaub HE, Kenny P, Ribi HO (1993) Monomeric and polymeric molecular films from diethylene glycol diamine pentacosadiynoic amide. J Phys Chem 97: 2928 – 2932

Weber J (1989) Nematocysts (stinging capsules of Cnidaria) as donnan-potential-dominated osmotic systems. Eur J Biochem 184: 465 – 476

Weber J, Klug M, Tardent P (1987) Some physical and chemical properties of purified nematocasts of Hydra Attenuata Pallas. Comp Biochem Physiol 88B: 855 – 862

Weisenhorn AL, Drake B, Prater CB, Gould SAC, Hansma PK, Ohnesorge F, Egger M, Heyn SP, Gaub HE (1990) Immobilized proteins in buffer imaged at molecular resolution by atomic force microscopy. Biophys J 58: 1251 – 1258